

RPA interacts with Rad52 to promote meiotic crossover and noncrossover recombination

Jeong H. Joo^{1,†}, Soogil Hong^{1,†}, Mika T. Higashide^{2,3}, Eui-Hwan Choi^{1,4}, Seobin Yoon¹,
Min-Su Lee¹, Hyun Ah Kang¹, Akira Shinohara^{1,2}, Nancy Kleckner⁵ and Keun P. Kim^{1,*}

¹Department of Life Sciences, Chung-Ang University, Seoul 06974, South Korea

²Institute for Protein Research, Graduate School of Science, Osaka University, Osaka 565-0871, Japan

³Current address: Graduate School of Engineering, Fukui University, Fukui 910-8507, Japan

⁴New Drug Development Center, Daegu-Gyeongbuk Medical Innovation Foundation, Deagu 41061, South Korea

⁵Department of Molecular and Cellular Biology, Harvard University, Cambridge 02138, USA

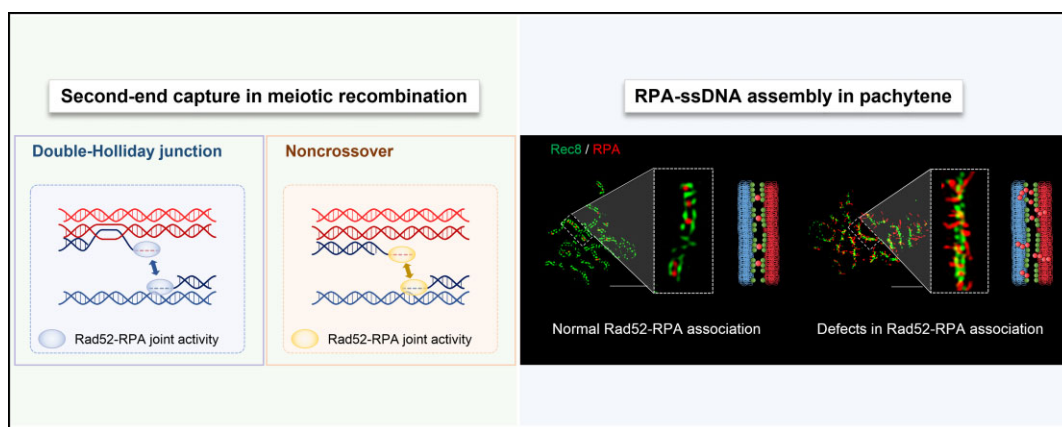
*To whom correspondence should be addressed. Tel: +82 2 820 5792; Fax: +82 2 820 5692; Email: kpkim@cau.ac.kr

†The first two authors should be regarded as Joint First Authors.

Abstract

Meiotic recombination is initiated by programmed double-strand breaks (DSBs). Studies in *Saccharomyces cerevisiae* have shown that, following rapid resection to generate 3' single-stranded DNA (ssDNA) tails, one DSB end engages a homolog partner chromatid and is extended by DNA synthesis, whereas the other end remains associated with its sister. Then, after regulated differentiation into crossover- and noncrossover-fated types, the second DSB end participates in the reaction by strand annealing with the extended first end, along both pathways. This second-end capture is dependent on Rad52, presumably via its known capacity to anneal two ssDNAs. Here, using physical analysis of DNA recombination, we demonstrate that this process is dependent on direct interaction of Rad52 with the ssDNA binding protein, replication protein A (RPA). Furthermore, the absence of this Rad52-RPA joint activity results in a cytologically-prominent RPA spike, which emerges from the homolog axes at sites of crossovers during the pachytene stage of the meiotic prophase. Our findings suggest that this spike represents the DSB end of a broken chromatid caused by either the displaced leading DSB end or the second DSB end, which has been unable to engage with the partner homolog-associated ssDNA. These and other results imply a close correspondence between Rad52-RPA roles in meiotic recombination and mitotic DSB repair.

Graphical abstract



Introduction

DNA recombination is a central feature of meiosis and, thereby, sexual reproduction (1,2). The DNA events of meiotic recombination, while elucidated primarily in budding yeast, are likely highly conserved across many organisms (1–3). Recombination initiates by programmed double-strand breaks (DSBs) which undergo endo- and exo-nucleolytic resection of their 5' ends to give long 3' single stranded (ss) DNA tails

(4–9). One of these tails interacts with the corresponding sequence on a homolog partner chromatid, making a nascent D-loop. The other end remains associated with its sister chromatid, likely also in nascent D-loop (10–12). At this point, the recombination process bifurcates. A few interactions are designated to give evenly spaced crossovers (COs) while most of the remaining interactions giving rise to noncrossovers (NCOs) (3,13–16). For CO-designated intermediates, nascent

Received: February 19, 2023. Revised: January 24, 2024. Editorial Decision: January 24, 2024. Accepted: January 27, 2024

© The Author(s) 2024. Published by Oxford University Press on behalf of Nucleic Acids Research.

This is an Open Access article distributed under the terms of the Creative Commons Attribution-NonCommercial License (<http://creativecommons.org/licenses/by-nc/4.0/>), which permits non-commercial re-use, distribution, and reproduction in any medium, provided the original work is properly cited. For commercial re-use, please contact journals.permissions@oup.com

D-loops first form a discrete long-lived ‘single end invasion’ intermediate (SEI) (10,13–15,17). The 3' tail of the leading DSB end is then extended by DNA synthesis (1). Then, in a critical transition, the lagging DSB end is released from its sister association and reanneals with the extended leading end ssDNA, an event known as ‘second end capture’ (18,19). Further events ultimately yield double-Holliday junctions (dHJs) which are matured to COs (17,20). NCO-designated intermediates also undergo extension of their 3' tails, but without a discrete identifiable intermediate (15,17). Among this branch of the pathway, it is the extended leading end that is released from the homolog partner, thus eliminating the interhomolog DNA connection (rather than the lagging end as for COs). But just as for COs, second end capture by strand annealing again occurs, with the released leading end being captured by the lagging DSB end to restore a non-exchange chromatid (20). Thus, strand annealing for second end capture is a critical feature of both branches of the recombination pathway. Finally, subsequent events produce mature NCO products without involvement of dHJs (15,20). DSBs, SEIs, dHJs, COs and NCOs are all detectable in two-dimensional gels (10,11,15,20).

The meiotic RecA homolog Dmc1 carries out strand exchange for both branches of the recombination pathway. The general RecA homolog Rad51 carries out strand exchange in mitotic cells but, in meiosis, is repurposed for two auxiliary roles (11,21–28). It accelerates loading of Dmc1 and it promotes preferential recombination with the homolog rather than the sister (‘homolog bias’) (11,27,28). Two other important players are RPA and Rad52. RPA is a prominent single strand binding protein. Thus far, RPA has been identified as having roles only in early steps: it binds to resected DSB ends, thereby blocking formation of inhibitory secondary structure, and may also bind to the ssDNA displaced at nascent D-loops (29–33). Rad52, instead, is known to act at both early and intermediate stages. The Rad52 subunit is composed of two distinct parts: a structured N-terminal half and a disordered C-terminal half. Using single-particle cryo-electron microscopy, it has recently been demonstrated that *S. cerevisiae* Rad52 functions as a homodecamer (34). Furthermore, the N-terminal half contains the primary DNA binding activity and oligomerization regions, while the C-terminal half contains the Rad51 and RPA binding motifs. Specifically, the C-terminal half contains a conserved region (residues 240–280) known as the ‘negative patch’, which is responsible for binding to RPA. In its early role, it displaces RPA from ssDNA ends to enable Rad51 loading, a function known as ‘mediator’ activity. [Other molecules play this mediator role for Dmc1] (18,35–41). Later, Rad52 provides the strand annealing activity responsible for the second end capture strand, along both the CO and NCO pathways (18). The distinction between the two roles of Rad52 is illustrated by the fact that a *rad52* mutant defective in mediator function exhibits very efficient formation of SEIs and dHJs (albeit with a defect in homolog bias due to failure of Rad51 loading) whereas, in contrast, a *rad52Δ* mutant, which lacks both mediator and strand annealing activity, exhibits a strong defect in progression from SEIs to dHJs, i.e. at the step where second end capture occurs (18).

Many lines of evidence show that Rad52 mediates second capture also for Rad51-promoted mitotic recombination (37,42–44). This process is known also to require RPA and, more specifically, to require direct interaction between Rad52 and RPA (45–47). Correspondingly, a *rfa1* mutant that specif-

ically abrogates the Rad52-RPA interaction, without affecting RPA-mediated single strand binding activity, is specifically defective for second end capture (37). These findings raised the possibility that the Rad52-RPA interaction might play an analogous role in meiosis, i.e. in Rad52-mediated second end capture for COs and/or NCOs, thereby defining a second role for RPA in this program.

To explore this possibility and, more generally, to further characterize the roles of the physical interaction between Rad52 and RPA, we have analyzed meiotic recombination *in vivo*, in budding yeast, in two mutants that disrupt that interaction: the previously analyzed *rfa1-t11* mutant and a reciprocal mutant of *RAD52*, *rad52-QDDD/AAAA*, that is not severely affected for strand annealing but is defective for interaction with RPA (45). Mutant phenotypes were defined by physical analysis of DNA events in synchronous cultures. Analysis of these ‘interaction-defective’ mutants was complemented by analogous analysis of the effects of timed degradation of RPA and Rad52. These studies show that abrogation of Rad52–RPA interaction confers a defect in progression from SEIs to dHJs which, along with other correlated defects, implies that this interaction is important for second end capture in meiotic recombination, for both COs and NCOs. The data also point to previously undetected role of RPA in dHJ resolution and hint at possible roles of Rad52–RPA interplay early in recombination, at the nascent D-loop stage. Finally, our study explored the interplay between RPA and Rad52 in persistent RPA–ssDNA filaments observed in *rfa1* and *rad52* mutants, which suppresses second end capture interaction and may be partially caused by defects in Rad52-mediated processes. Therefore, our findings demonstrated the involvement of RPA in a previously unidentified pathway in the meiotic recombination process. Overall, these findings extend the significant analogies between mitotic and meiotic DSB-initiated recombination.

Materials and methods

Strains

Detailed information on strain genotypes and characteristics can be found in **Supplementary Table S1**. The *HIS4LEU2* locus has been described in (17).

Meiotic time course

All yeast strains used in our experiments were isogenic derivatives of diploid *Saccharomyces cerevisiae* strain SK1 (**Supplementary Table S1**). Diploid cells were grown in YPG medium (1% (w/v) yeast extract, 2% (w/v) bacto-peptone, 3% glycerol, and 2% (w/v) bacto-agar) for 18 h. The grown cells were streaked on YPD (1% (w/v) yeast extract, 2% (w/v) bacto-peptone, 2% (w/v) dextrose, and 2% (w/v) bacto-agar). Two days later, a single colony was inoculated into 2 ml liquid YPD medium (1% (w/v) yeast extract, 2% (w/v) bacto-peptone, and 2% (w/v) dextrose) and cultured for 24 h in a shaking incubator. To synchronize cells in the G₁ phase, the cultured cells were diluted to pre-warmed supplemented pre-sporulation medium (SPS; 1% (w/v) potassium acetate, 1% (w/v) bacto-peptone, 0.5% (w/v) yeast extract, 0.67% (w/v) yeast nitrogen base without amino acids, 0.5% (w/v) ammonium sulfate, 0.05 M potassium biphthalate, adjusted pH to 5.5). The cells were washed with pre-warmed sporulation medium (SPM; 1% (w/v) potassium acetate, 0.02%

(w/v) raffinose, and 0.015% (v/v) antifoam) and were induced into meiosis in SPM at 30°C. The cell samples were then harvested at each time point and treated with trioxalen to crosslink on UV light at 365 nm (6 mW/cm²) for 10 min. For the analysis of meiotic cell division, cells were fixed with 40% ethanol and 0.1 M sorbitol and stained with 4',6-diamidino-2-phenylindole (DAPI). For analysis of *RAD52-AID* or *RFA1-AID* cells, 30 μM CuSO₄ was added to induce expression of OsTIR1 under the control of copper-inducible promoter (pCUP1) after 2 h. After induction of meiosis, DMSO or 2 mM 3-indoleacetic acid (auxin) was added in the culture at 2.5 h. Protein depletion was verified by western blot analysis.

DNA physical analysis

DNA physical analysis was performed as previously described (10,11,48–51). For one-dimensional (1D) gel analysis, 2 μg of genomic DNA was digested with XhoI restriction enzyme for 3 h at 37°C. The DNA samples were then loaded onto a 0.6% UltraKem LE agarose gel in TBE buffer (89 mM Tris, 89 mM boric acid, 2 mM EDTA, pH 8.0) without ethidium bromide (EtBr) at approximately 2 V/cm for 24 h. For two-dimensional (2D) gel analysis, the first gel was prepared with 0.4% agarose in TBE buffer without EtBr at approximately 1 V/cm for 21 h and stained with 0.5 μg/ml EtBr in TBE for 30 min. The gel was then sliced from the top to the 1 kb DNA marker and transferred to 2D gel trays. The DNA species of the 2D gel were separated in 0.8% UltraKem LE agarose gel in TBE with 0.5 μg/ml EtBr. For the analysis of COs and NCOs in the 2D gel, 2 μg of genomic DNA was digested with XhoI. The DNA samples were loaded onto a 0.6% gold agarose gel in TBE buffer without EtBr and separated via electrophoresis at approximately 1.5 V/cm for 24 h. The gel was stained with 0.5 μg/ml EtBr in TBE for 30 min, after which the gels were sliced from 7 kb to 3 kb. The gel stripes were washed with 10 mM Tris-Cl (pH 8.0) for 30 min and incubated with BamHI buffer without BSA for 15 min. The BamHI enzyme was added to the BamHI buffer with 0.1 mg/ml BSA and the gel strips were incubated overnight at 37°C. The DNA species of the 2D gel were separated in a 0.7% UltraKem LE agarose gel in TBE without EtBr. Southern blot hybridization was conducted as described previously (10,52).

Yeast chromosome spreading and immunofluorescence imaging

Chromosome spreads for immunofluorescence analysis were prepared as described previously (50,52–54). Cells at each time point were resuspended in ZK buffer (50 mM Tris-Cl, 0.5 M KCl, pH 7.5) followed by dithiothreitol treatment (DTT; final concentration = 25 mM) for 2 min at room temperature. The cells were harvested and resuspended in 0.4 ml ZK buffer with 3 μl of 100T zymolyase treatment for each sample. Cells were obtained by centrifugation and washed once with 1 ml MES solution. A proper number of cells in MES solution were dropped on a slide glass, after which they were sequentially treated with 30 μl paraformaldehyde solution and 80 μl 1% Lipsol. After allowing the samples to air dry overnight, the slide glasses were dipped in 0.2% Photo-Flo (Kodak Ltd) for 30 s. The samples were then air dried once again and the slide glasses were transferred to TBS buffer (20 mM Tris-Cl, 136 mM NaCl, 3 mM KCl; pH 7.5) for 15 min. The following antibodies were used in this study for immunostaining: rabbit polyclonal RPA antibody (diluted

1:1000; Agrisera, AS-07214); guinea pig polyclonal Rad51 antibody (diluted 1:200; 54); rabbit polyclonal Dmc1 antibody (diluted 1:200; 54); rat polyclonal myc antibody (diluted 1:400; Biorad, MCA1929); mouse monoclonal myc antibody (diluted 1:400; Santa Cruz Biotechnology, sc-40); mouse monoclonal HA antibody (diluted 1:400, Santa Cruz Biotechnology, SC-7392); Alexa-fluor-488 conjugated goat anti-mouse IgG (diluted 1:300; Jackson Immuno Research, 115-545-003); TRITC conjugated goat anti-rabbit IgG (diluted 1:300; Jackson Immuno Research, 111-025-003); Alexa-fluor-647 conjugated goat anti rat IgG (diluted 1:300; Jackson Immuno Research, 112-605-003); Alexa-fluor-647 conjugated goat anti guinea pig IgG (diluted 1:300; Jackson Immuno Research, 106-605-003). Images were captured using a fluorescence microscope (Nikon Eclipse Ti) and a microscope camera (Nikon DS-Qi2). Super-resolution images of chromosome spread were acquired using a Nikon Eclipse Structured Illumination Microscopy (SIM) imaging system equipped with an EM CCD camera iXon897 (100× Plan Apochromat lens, 1.49 NA). Images were processed and assembled into figures using the Nikon NIS-Elements platform.

In vitro protein interaction analysis

The plasmids pGEX-KG-RAD52, pET16b-RFA1, pET16b-rfa1-K45E and pET16b-rfa1-K45A were transformed into BL21(DE3) cells for protein expression. The BL21(DE3) cells were cultured in LB medium supplemented with 0.1 mg/ml ampicillin at 37°C until reaching an optical density (OD₆₀₀) of 0.5–0.6. Protein expression was induced by adding 0.5 mM isopropyl-β-D-1-thiogalactopyranoside at 30°C for 20 h. For cell lysis, the induced cells were resuspended in lysis buffer (20 mM Tris-Cl, pH 7.5, 100 mM NaCl, 1 mM EDTA, protease inhibitor cocktail, and 0.5 mM phenylmethylsulfonyl fluoride). Cell lysis was achieved by incubation with 0.4 mg/ml lysozyme at 4°C followed by sonication. Subsequently, Rad52 and RPA proteins were co-purified using glutathione agarose resin and Ni-NTA agarose resin, respectively. Interactions between the proteins were visualized by staining the gel with Coomassie Blue.

Co-immunoprecipitation assay

Yeast cell extraction and immunoprecipitation were performed as described previously (55). Cells were harvested and washed with cold TBS buffer (20 mM Tris-Cl, 136 mM NaCl, 3 mM KCl; pH 7.5). The cells were then resuspended in 600 μl of lysis buffer (120 mM NaCl, 50 mM Tris-Cl (pH 7.5), 0.1% NP-40, 10% glycerol, 5 mM EDTA (pH 8.0), 0.5 mM phenylmethylsulfonylfluoride) with EDTA-free protease inhibitor (Roche, 111873580001). The cells were disrupted with a bead beater using 0.5 mm acid-washed glass beads (Sigma, G8772). For the immunoprecipitation of Rad52-9myc, 1 mg of proteins was incubated overnight with mouse monoclonal myc antibodies (Santa Cruz Biotechnology, SC-40). Pre-washed protein A/G beads (20 μl; Gendepot, P9203) were added to the cell extract and the mixture was incubated for 3 h. The protein A/G beads were then harvested by centrifugation at 3000 rpm. The beads were washed three times with 600 μl lysis buffer with EDTA-free protease inhibitor. The beads were then mixed with 20 μl SDS-PAGE gel sample buffer and boiled at 95°C for 5 min. The following antibodies were used in this study for immunoblotting: mouse monoclonal myc antibody (Santa Cruz Biotechnology, SC-40);

rabbit polyclonal RPA antibody (Agrisera, AS-07214); mouse monoclonal Pgk1 antibody (Invitrogen, 459250); Peroxidase AffiniPure Goat anti-mouse IgG (H + L) (Jackson Immuno Research, 115-035-003); Peroxidase AffiniPure Goat anti-rabbit IgG (H + L) (Jackson Immuno Research, 111-035-003). The membranes were observed using a ChemiDoc MP imaging system (Bio-Rad).

Physical analysis of mitotic recombination

To synchronize cells in the G₁ phase, diploid cells were cultured in SPS for 18 h at 30°C. The cells were then transferred to YPG medium (1% (w/v) bacto yeast extract, 2% (w/v) bacto peptone, and 2% (w/v) galactose) to induce I-SceI expression. Afterward, the cells expressed I-SceI endonuclease from the GAL promoter generating DSBs at the I-SceI restriction enzyme sites. To repress I-SceI expression, 3% glucose was added to each culture at 45 min.

Mouse chromosome spreading and immunofluorescence cytology

Chromosome spreads for immunofluorescence analysis were prepared as described previously (56). The following primary antibodies were used in this study for immunostaining: monoclonal mouse SYCP3 antibody (diluted 1:500, Santa Cruz Biotechnology, SC-74569); polyclonal rat RPA antibody (diluted 1:200, Cell signaling, 2208). The following are the secondary antibodies were used in this study: FITC conjugated goat anti-rat IgG (diluted 1:500, Jackson Immuno Research, 112-095-003); TRITC conjugated goat anti-mouse IgG (diluted 1:500, Jackson Immuno Research, 115-025-003). Images were captured using a Super resolution microscope (Nikon Eclipse Ti) equipped with an EM CCD camera (iXon897, 100× Plan Apochromat lens, 1.49 NA). Images were deconvoluted and assembled into figures with the Nikon NIS software.

Chromatin immunoprecipitation

Chromatin immunoprecipitation (ChIP) analysis was conducted to characterize the *HIS4LEU2* locus (57). Cells were fixed by addition of 1% formaldehyde for 20 min, followed by quenching with 125 mM glycine for 5 min at room temperature. The cells were lysed with acid-washed glass beads, and the cell extracts were sonicated to fragment the genomic DNA to an average length of 500 bp. The extracts were incubated with anti-Rfa1 overnight and bound to protein A-magnetic beads for 2 h. The beads were recovered and thoroughly washed. Samples containing protein-bound DNA were treated with proteinase K followed by phenol extraction/ethanol precipitation. The PCR mixture contained Taq buffer, DNA polymerase, 2.5 mM of dNTPs, an appropriate set of primers, and input and ChIP DNA samples from each time point as templates. Input samples were used as a standard. The specific primers for the *HIS4LEU2* and *SMC1* locus were following: For *HIS4LEU2* locus, 5'-GACACCAGAGTTCAAATTCCAACGAG-3' and 5'-CCAGCAGTTATTTATACTTGCAGCATC-3'; for *SMC1* locus, 5'-GGTGTGCGGAGTAATCATTGAGG-3' and 5'-TTATAGGAGACAGTTTCATCAA-3'. The extent of amplification was empirically determined to avoid saturation of the amplified bands. To quantify the PCR products, each sample was separated via electrophoresis in 1.2% agarose gel and

stained with EtBr. The amplified DNA bands were quantified with the ImageJ software (NIH Image).

Statistical analysis

All statistical calculations were performed using the prism software (GraphPad). All figures representing data are shown as mean values, with error bar (S.D.), as shown in the figure legends. The numbers of biological replicates used for representing data were detailed in each figure legends.

Results

Interaction-defective mutants of RPA and Rad52

Previous studies have identified separation of function mutations of RPA and Rad52 which retain their basic activities but are defective in their mutual interaction (45,46). The *rfa1-t11* mutation (*rfa1-K45E*) maps to the N-terminal OB fold of Rfa1, the largest subunit of RPA (31,58). In *in vitro* analysis of Rad51-mediated (mitotic) recombination, the *rfa1-t11* protein retains normal single strand binding but is defective in interaction with Rad52 (37,59) and, correspondingly, is defective in Rad52-mediated second end capture (Introduction). The *rfa1-t11* mutation disrupts a critical basic patch within the binding pocket of the N-terminal OB fold, causing the K45E residue to protrude into the binding cleft (58,60). *In vitro* protein binding analysis, we observed that Rfa1 proteins carrying glutamic acid or alanine substitution of K45 are defective in protein-protein interaction to Rad52 (Supplementary Figure S1). Analogously, the Rad52-Q275A/D276A/D277A/D278A mutant (herein *rad52**) retains normal interaction with Rad51 and normal DNA annealing activities but is partially deficient in binding RPA (45) (Figure 1A and B, Supplementary Figures S1 and S16).

For the present study, we confirmed the expected defects in physical interaction of Rad52 and Rfa1 *in vivo*. The two single mutants confer significant effects and the *rfa1-t11 rad52** double mutant exhibits more severe defects than either single mutant strain (Supplementary Figures S1 and S16). Interestingly, the same hierarchy is also seen for several basic phenotypes including: (i) timing and efficiency of the meiotic divisions; (ii) final level of viable spores at 24 h (Figure 1C); (iii) spore viability (Figure 1D); and (iv) physical interaction between wild type (WT) and mutant forms of Rfa1 and Rad52 (Supplementary Figures S1 and S16). We also demonstrate by cytological analysis that both single mutants and the double mutant all exhibit WT levels of Rad51 foci at pachytene, implying that, as anticipated, Rad52 mediator function is intact, *in vivo*, in all three mutants (Supplementary Figure S2).

Recombination defects in interaction-defective mutants correspond to those expected for defective second end capture

To assess the nature of meiotic recombination conferred by *rfa1-t11* and *rad52** mutations, we constructed diploid mutant strains containing a *HIS4LEU2* locus hotspot and analyzed their molecular functions through physical analysis of meiotic recombination as a function of time after initiation of meiosis in synchronous cultures (Figure 1E).

DSBs

DSBs and COs were monitored in one-dimensional (1D) gels. In WT meiosis, DSBs appear at 2.5 h and disappear over time,

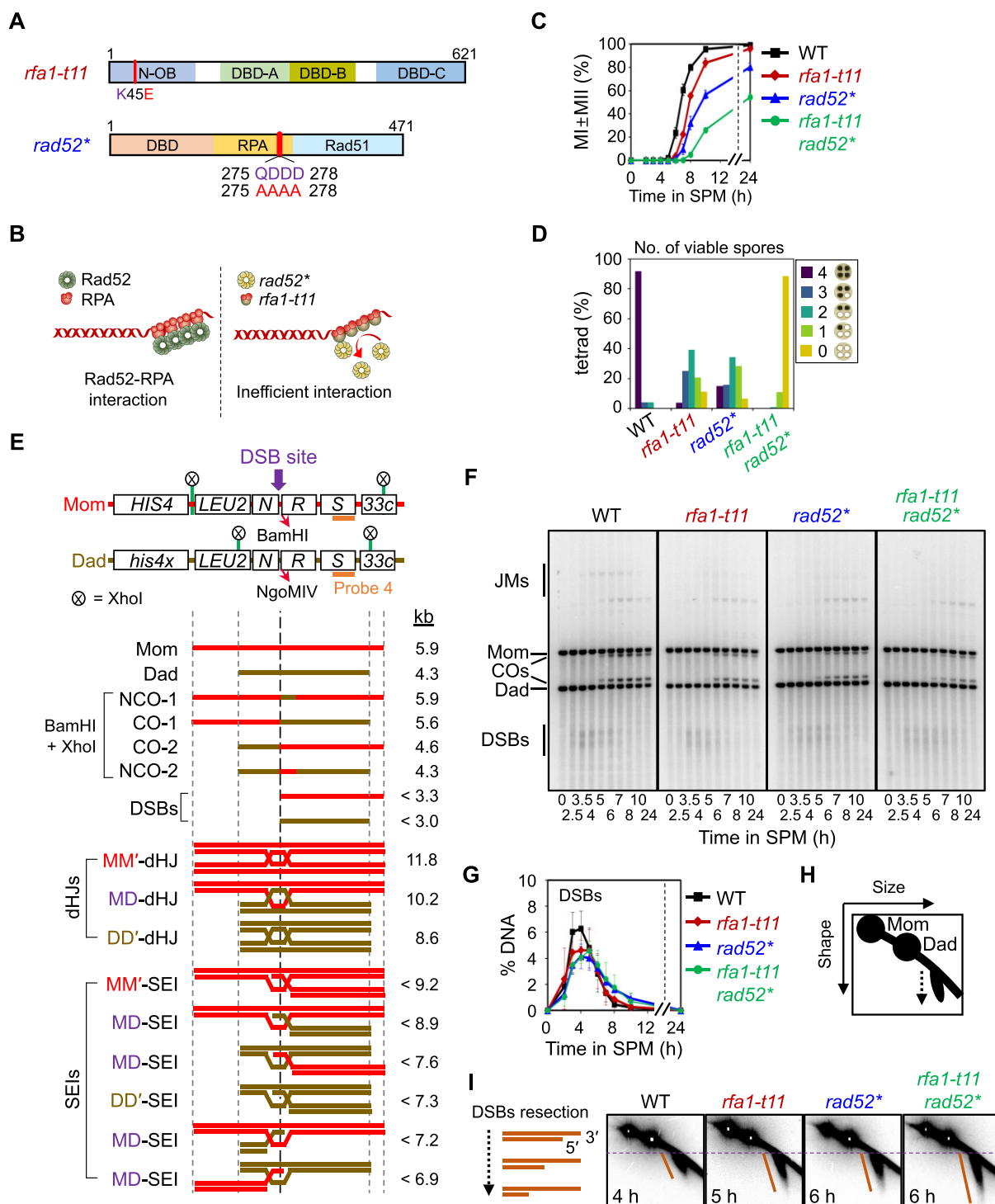


Figure 1. *rfa1-t11* and *rad52** cells exhibit defects in meiotic progression. **(A)** Schematic diagram of Rfa1 with a point mutation at the OB domains and Rad52 with an RPA binding domain. The red line indicates the *rfa1*-K45E single mutation, resulting in effective DNA replication but strongly deficient recombination (85). *rad52** indicates QDDD-275-278-AAAA mutation in the RPA interaction domain. The positions of the indicated amino acid changes are illustrated in each domain. N-OB, N-terminal oligonucleotide/oligosaccharide binding; DBD, DNA binding domain; RPA, RPA binding domain; Rad51, Rad51 binding domain. **(B)** Rad52 and Rfa1 mutants analyzed in this study and schematic cartoon of Rad52 and Rfa1, including previously reported mutants with known phenotypes (37,45,46). **(C)** Meiotic nuclear division in WT and mutants. The data represent the mean \pm SD ($N > 200$ for each time point; three independent biological replicates). **(D)** Distribution of viable spores in WT and mutants. **(E)** Physical map of *HIS4/LEU2* locus of chromosome III showing diagnostic restriction enzyme sites and position of Probe 4. CO-1, crossover-1 (5.6 kb); CO-2, crossover-2 (4.6 kb); NCO-1, noncrossover-1 (5.9 kb); NCO-2, noncrossover-2 (4.3 kb); DSBs, double-strand breaks (<3.3 and <3.0 kb); SEI, single-end invasion; dHJ, double-Holliday junction. **(F)** One dimensional gel (1D gel) analysis in WT, *rfa1-t11*, *rad52** and *rfa1-t11* *rad52** strains. **(G)** Quantification of the DSBs shown in (F). Data are presented as the mean \pm SD ($N = 3$). **(H)** Two-dimensional (2D) gel displaying parental and DSB species. **(I)** 2D gel detection of DSB resection: images from the time point of maximum abundance.

followed by appearance of COs (WT in Figure 1F). DSBs appear and disappear with similar timing and with similar state levels in WT and *rfa1-t11*, but with a slight decrease in maximum levels and with a minority of DSBs remaining present at later-than-normal times (Figure 1G). Resection of 5' DSB ends was monitored in two-dimensional (2D) gels. All three mutants exhibit significant hyperresection as compared to WT, with more extensive resection in the double mutant than in either single mutant (Figure 1H and I).

SEIs and dHJs

Formation and disappearance of the two CO-specific intermediates, SEIs and dHJs, (Introduction) can be monitored by 2D gel analysis. For dHJs, interactions between homologs can be distinguished from interactions between sister chromatids (Figure 2A). In WT meiosis, SEIs and dHJs appear and disappear sequentially (Figure 2B and C, Supplementary Figure S3). IS-dHJs and IH-dHJs occur with very similar kinetics but with a substantial excess of IH-dHJs (IH:IS dHJ ratio of ~5.5:1) reflecting the intrinsic bias of meiotic recombination for homolog partners over sister partners (WT in Figure 2C).

In all three interaction-defective mutants, SEIs and dHJs, of both types, appear and disappear, but with a delay of ~2 h relative to WT (Figure 2C). Since most DSBs appear and disappear in a timely fashion, this kinetics imply a delay of ~2 h at the DSB-to-SEI transition. The basis for this defect is not clear. No such defect was reported for a mediator-defective Rad52 mutant and this defect arises before second end capture. One possibility is that Rad52-RPA interaction plays an unsuspected early role after Rad51 loading, in the formation of nascent D-loops, in accord with evidence that RPA may localize to the displaced strand in these structures (61,62).

Most strikingly, all three mutants exhibit only a modest reduction in the level of SEIs but a dramatic reduction in the level of total dHJs ($1.1 \pm 0.2\%$ for WT versus $0.54 \pm 0.2\%$ for *rfa1-t11*, $0.68 \pm 0.3\%$ for *rad52** and $0.52 \pm 0.1\%$ for *rfa1-t11 rad52**) (Figure 2C). This disparity directly implies a defect in progression from SEIs to dHJs along the interhomolog CO pathway, as defined previously for Rad52 alone (18), and thus, by implication, a role for Rad52-RPA interaction in second end capture. There is also a differential effect on IH- versus IS-dHJs, which remain relatively unaffected (Figure 2C). This distinction remains to be understood but might be a secondary consequence of the second end capture defect.

COs and NCOs

Occurrence of CO and NCO recombination products can be assessed very sensitively by appropriate 2D gel analysis (16,18). All three interaction-defective mutants show reduced levels of both types of products, with a greater reduction in NCOs as compared to COs (Figure 2E). Analogously to DSB phenotypes, this phenotype is not observed in a *rad52* mutant defective only in mediator activity, where COs and NCOs are reduced to the same extent, but is observed in *rad52Δ*, where NCOs are also differentially reduced (18). It can thus be attributed to an activity downstream of mediator function that is carried out jointly by interacting Rad52 and RPA. This difference has been attributed previously to a defect in second end capture: a CO-fated event that fails in this step still retains its first end/partner interaction and thus can yield ‘half crossover’ products whereas NCO-fated events lose their first end/partner interaction and, without second end capture,

cannot yield such products (18; Discussion). The CO defects shown in the mutants are also consistent with the results of the mitotic recombination assay (Supplementary Figure S4).

Timed degradation of Rad52, or of RPA, implicate both molecules individually in second end capture

As another probe for the roles of these molecules in second end capture, we initiated their degradation at a time in meiosis when SEI formation has just begun. At this time, most recombination intermediates will have carried out the early roles of both Rad52 and RPA for Rad51 loading and nascent D-loop formation but will not have proceeded as far as second end capture. Thus, effects of degradation observed in this protocol are expected to reflect role(s) of the degraded molecule in intermediate and later steps of recombination. Auxin-inducible degron constructs for the two proteins were used for this analysis, with degradation initiated by addition of auxin.

Rad52

Timed degradation of Rad52 confers the effects predicted to reflect absence of second end capture as described above: efficient SEI formation and disappearance; a dramatic reduction in total dHJs, with a differential effect on IH-dHJs; and a reduction in both COs and NCOs, with a differential reduction of NCOs (Figure 3A, C, E and G, Supplementary Figure S5).

Rad52 in rfa1-t11

In a *rfa1-t11* background, the phenotypes diagnostic of defective second end capture are apparent, as described above; however, direct comparison shows that these effects are less severe than those conferred by *rad52Δ* (Figures 2 and 3A, C, E and G, Supplementary Figure S5). Accordingly, timed degradation of Rad52 in an *rfa1-t11* background increases the severity of the effects to those seen in *rad52Δ* (Figure 3A, C, E and G).

Rfa1

Timed degradation of Rfa1 alone also has dramatic effects. The level of SEIs continues to increase to very high levels, reaching more than twice the maximum level observed in the absence of degradation, implying a complete block in progression to dHJs (Figure 3B and D, Supplementary Figure S5). The level of dHJs also increases and a few CO/NCO products form, presumably due to progression of SEIs formed prior to degradation. However, the two phenotypes diagnostic of a second end capture defect are again observed, i.e. a differential deficit of IH-dHJs relative to IS-dHJs, and a differential reduction in NCOs relative to COs (Figure 3B, D, F and H, Supplementary Figure S5). Importantly, the *RAD52* gene is unaltered in this experiment. Thus, these findings provide strong additional evidence that RPA plays a direct role in second end capture. Finally, in this protocol, dHJ levels increase to a certain point and then plateau. This phenotype suggests that RPA is required for dHJ resolution (Figure 3B and D, Supplementary Figure S5). This role has not previously been detected (Discussion).

RPA/Rad52 interaction mutants exhibit spikes of RPA at CO sites

RPA signals occur prominently along WT meiotic prophase chromosomes of several organisms, including as bridges

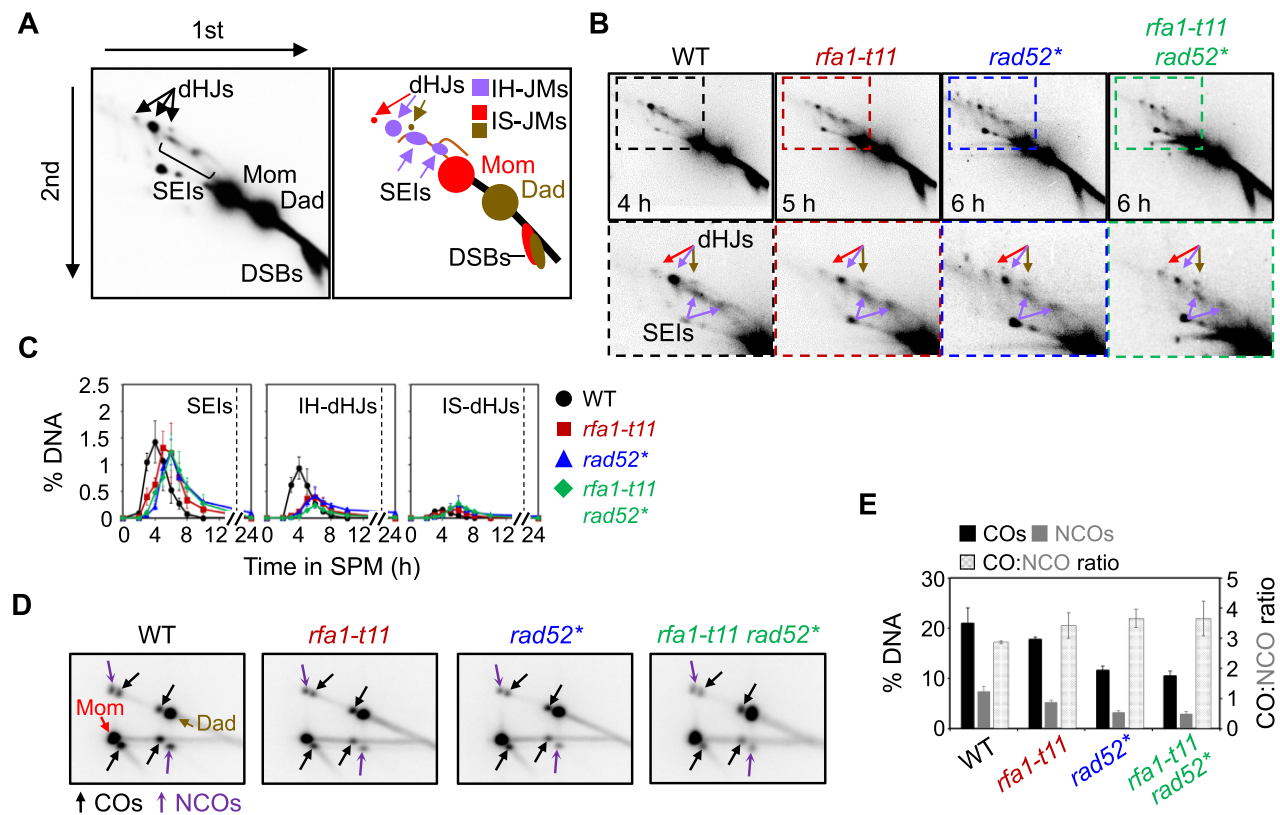


Figure 2. SEI-to-dHJ transition is inefficient in *rfa1-t11* and *rad52**. **(A)** Illustration of 2D gel. IH-JM, MM' IS-JM and DD' IS-JM species are shown in purple, red and brown, respectively. dHJ, double-Holliday junction; SEI, single-end invasion; DSBs, double-strand breaks. **(B)** Two-dimensional gel (2D gel) analysis in WT, *rfa1-t11*, *rad52** and *rfa1-t11 rad52** strains. The positions of SEIs and dHJs are indicated by arrows. Red arrows, MM' IS-dHJs; brown arrows, DD' IS-dHJs; purple arrows, MD IH-JMs. **(C)** Quantification of SEIs and dHJs. Data are presented as the mean \pm SD ($N = 3$). **(D)** CO and NCO two-dimensional gel analysis in WT, *rfa1-t11*, *rad52** and *rfa1-t11 rad52** strains at peak time. Representative images showing the maximum levels of CO and NCO species. Black arrow, COs; purple arrow, NCOs. **(E)** Quantification of the COs and NCOs shown in (D). Data are presented as the mean \pm SD ($N = 3$). Black bar, COs; gray bar, NCOs.

that link homolog axes even prior to SC formation (63) (Supplementary Figure S6). For the present study, we examined the localization of RPA signals along spread yeast pachytene chromosomes in which chromosome axes were simultaneously visualized by staining with RPA and meiotic cohesin Rec8, a prominent axis component. In WT, RPA signals can be observed as linkages between the coaligned pachytene axes, as in other cases (Figure 4A and B, Supplementary Figure S7). Four lines of evidence imply that the signals detected in the present study correspond specifically to the sites of CO-fated recombination interactions. (i) They appear at about the time of CO-related SEIs (~ 4 h). (ii) They occur normally in the absence of SC formation (in a *zip1Δ* mutant) (Figure 4C, Supplementary Figure S8), as CO-correlated recombination complexes are known to do (64). (iii) They require Spo11 (and thus DSBs to initiate recombination) cases (Figure 4D). And most directly, (iv) they strongly colocalize with foci of the SUMO E3 ligase Zip3 (Figure 5A–C), which is known to specifically mark the sites of COs (64–71).

Dramatically, in all three interaction-defective mutants, prominent RPA signals are again present, but now occur as elongated ‘spikes’ that emerge from one or the other homolog axis (Figures 4B and 5D). These spikes appear at the same time as RPA signals in WT; are again dependent on Spo11 and independent of SC formation/Zip1; and strongly colocalize with

Zip3 foci (Figures 4 and 5). Thus, they appear to reflect aberrant status of CO-fated recombination intermediates. However, in contrast to the RPA bridges seen in WT signals which disappear in later stages of meiosis, RPA spikes in interaction mutants accumulate to, and remain at, high levels, implying a defect in turnover (Figure 4D). To monitor the binding of RPA to DSB/recombination sites, chromatin immunoprecipitation (ChIP) assays were conducted on strains carrying the *HIS4LEU2* hotspot, characterized by a very high DSB frequency. In the WT, RPA was recruited to the locus from 2 h, and RPA binding peaked at 4–6 h (the time at which high levels of joint molecules are present) (Supplementary Figure S9). However, *rfa1-t11*, *rad52** and *rfa1-t11 rad52** cells exhibited an impaired turnover of RPA binding, with a > 2 h delay, suggesting that RPA prolongs the binding of ssDNA on meiotic recombination sites (Supplementary Figure S9).

Spikes with analogous morphology and analogously defective turnover are also observed after timed degradation of Rad52 in both WT and *rfa1-t11* backgrounds (Figure 6, Supplementary Figures S10, S11 and S17). Furthermore, regions of abundance for long RPA-ssDNA filaments are often depleted for cohesin throughout the chromosomes (Figure 6E). Similar SIM imaging data were obtained for *rad52Δ* (Supplementary Figure S12). Given the elongated nature of the RPA signals in the mutant and the fact that RPA should mark segments of ssDNA, these signals should comprise

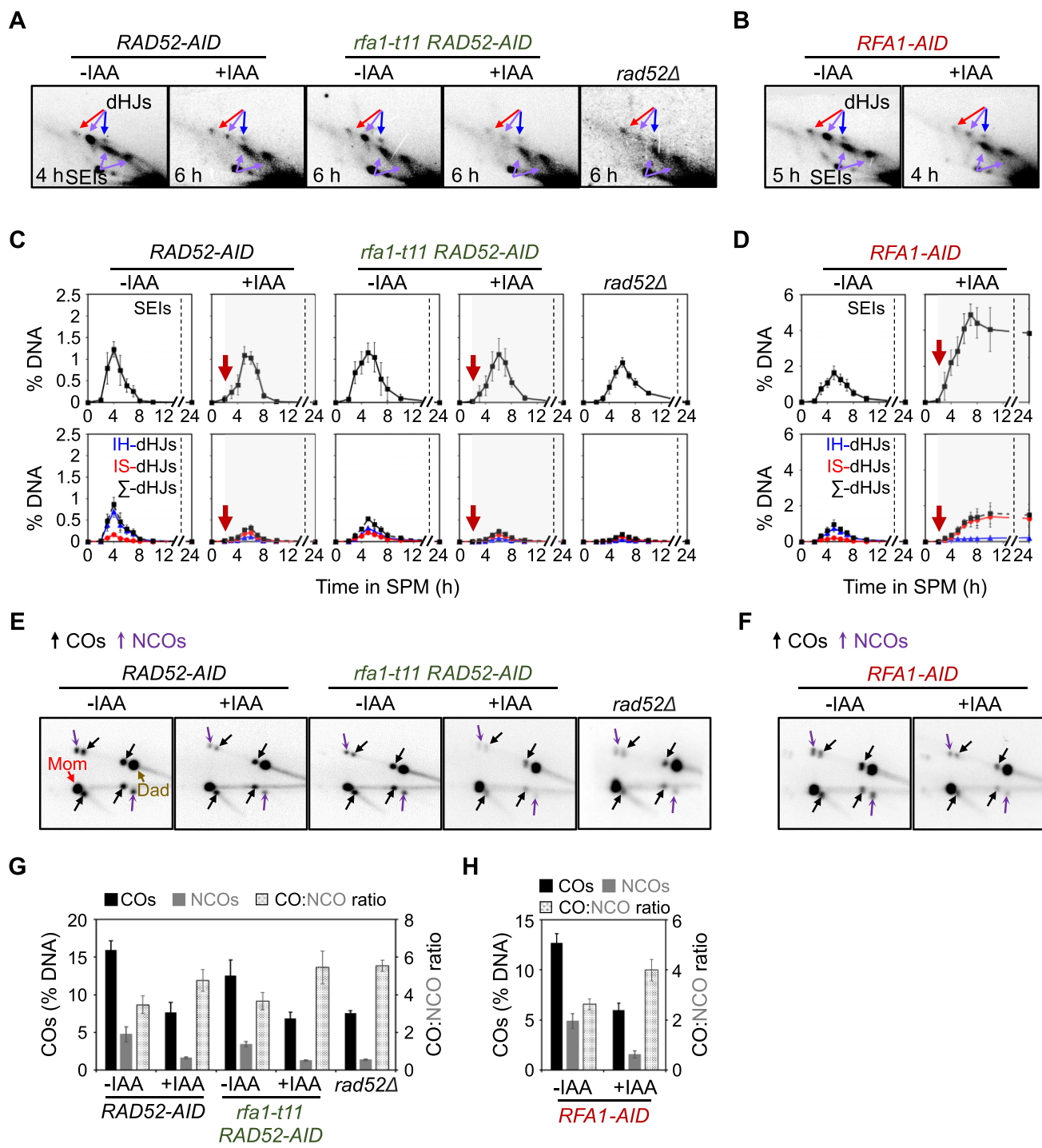


Figure 3. Both RPA and Rad52 are required to promote post-invasion steps. **(A, B)** Representative images of 2D gels at the time point of maximum level in (C) [except for *RFA1-AID* (+IAA) gel image (4 h)]. The positions of SEIs and dHJs are indicated by arrows. Red arrows, MM' IS-JMs; blue arrows, DD' IS-JMs; purple arrows, MD IH-JMs. **(C, D)** Quantification of SEIs and dHJs in *RAD52-AID*, *rfa1-t11 RAD52-AID*, *RFA1-AID* and *rad52Δ* strains. Auxin (2 mM) was added to induce degradation of Rad52 or Rfa1 at 2.5 h (red arrow). Data are presented as the mean \pm SD ($N = 3$). **(E, F)** Representative image of CO and NCO 2D gel analysis. **(G, H)** Quantitative analysis of the COs and NCOs shown in (E, F). Auxin (2 mM) was added to induce degradation of Rad52 or Rfa1 at 2.5 h. Data are presented as the mean \pm SD ($N = 3$). Black bar, COs; gray bar, NCOs.

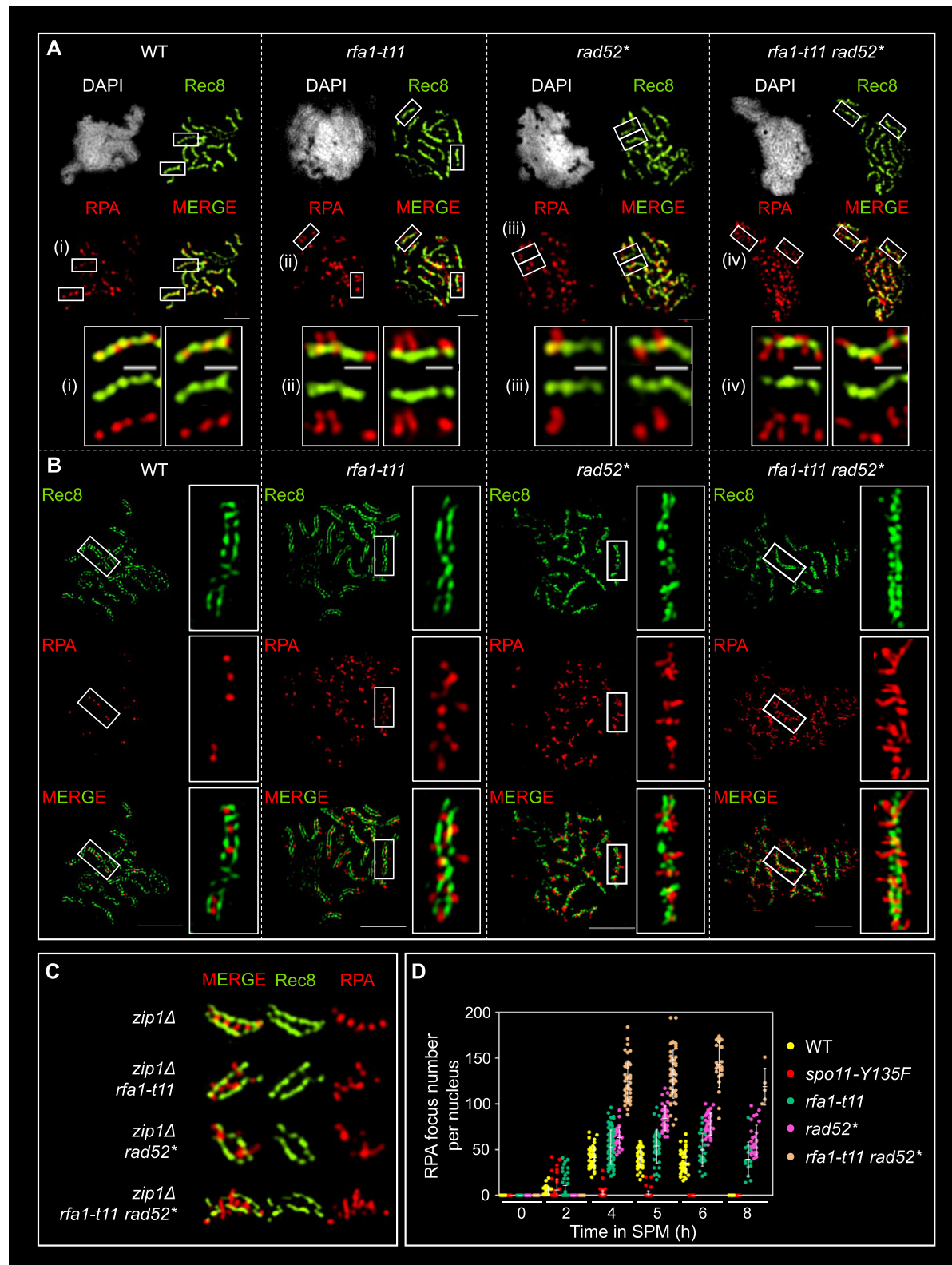


Figure 4. Localization of RPA-single stranded DNA in WT, *rfa1-t11*, *rad52** and *rfa1-t11 rad52** cells. **(A)** Immunofluorescence analysis of a meiotic nuclear spread of WT, *rfa1-t11*, *rad52** and *rfa1-t11 rad52**. The cells were stained for anti-Rfa1 (Red) and anti-HA (Green). The scale bar represents 2.5 μ m. (i-iv) The boxed regions at the bottom of each panel are magnified images. The scale bar of magnified images represents 1 μ m. **(B)** Representative structured illumination microscopy (SIM) images of WT (4 h), *rfa1-t11* (4 h), *rad52** (5 h) and *rfa1-t11 rad52** (6 h) mutant chromosomes. The cells were stained for Rec8 (Green) and Rfa1 (Red). The scale bar represents 2.5 μ m. Enlarged images of the boxed regions are shown to the right of each panel. **(C)** Immunofluorescence analysis of a meiotic nuclear spread in *zip1 Δ* , *zip1 Δ rfa1-t11*, *zip1 Δ rad52** and *zip1 Δ rfa1-t11 rad52**. The cells were stained for Rec8 (Green) and Rfa1 (Red). **(D)** Number of RPA foci per nucleus in the WT, *spo11-Y135F*, *rfa1-t11*, *rad52** and *rfa1-t11 rad52** strains. Data are presented as the mean \pm SD ($N \geq 20$).

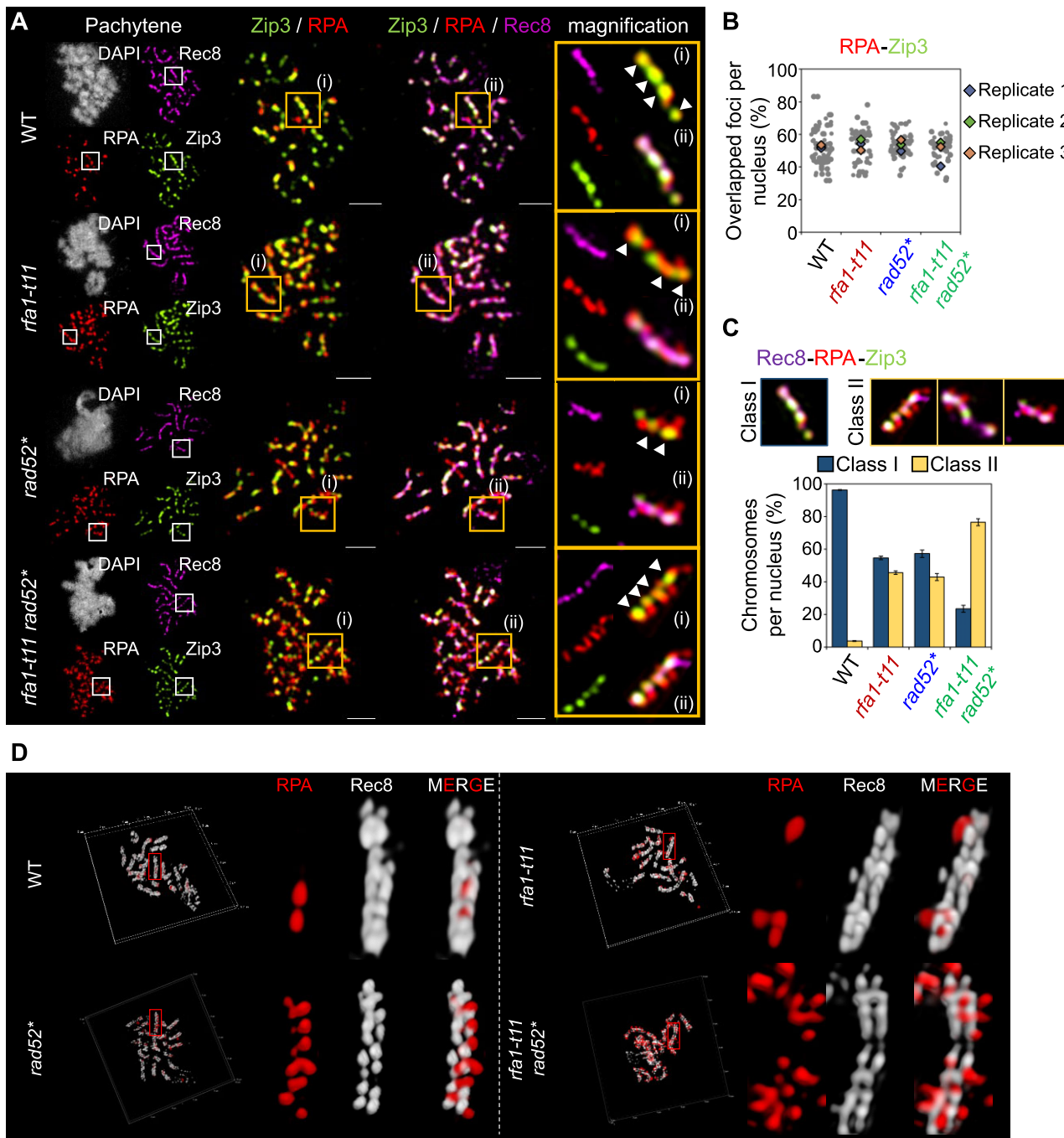


Figure 5. Recruitment of RPA to the recombination sites. **(A)** Immunofluorescence analysis of a meiotic nuclear spread in the WT, *rfa1-t11*, *rad52** and *rfa1-t11 rad52** strains. The cells were immunostained with anti-RPA, anti-myc (for Zip3-13myc) and anti-HA (for Rec8-3HA) antibodies. The scale bar represents 2.5 μ m. Right panel: (i) RPA-Zip3 staining images; (ii) Rec8-RPA-Zip3 staining images. White arrow heads indicate overlapped Rfa1-Zip3 foci. **(B)** Quantification of RPA-Zip3 overlap foci per nucleus at the time point of maximum level in WT, *rfa1-t11*, *rad52** and *rfa1-t11 rad52** shown in (A). **(C)** Classification of RPA-Zip3 staining on chromosome axis. Top: Classification of chromosomes. Class I, overlapped RPA-Zip3 foci; Class II, overlapped RPA-Zip3 foci with Rfa1 spike signal. Bottom: percentage of class I and class II chromosomes in WT, *rfa1-t11*, *rad52** and *rfa1-t11 rad52**. **(D)** Representative 3D SIM z-stack images of a pachytene chromosome immunostained with anti-RPA and anti-HA (for Rec8-3HA) antibodies.

resected ssDNA ends. This possibility is supported by examination of the effects of eliminating the nuclelease responsible for resection in an Exo1-nuclease dead allele (*exo1-D173A*; 9) using SIM images. No long spike RPA filaments were detected in *exo1-D173A rfa1-t11*, *exo1-D173A rad52** and *exo1-D173A rfa1-t11 rad52**. However, there were still large numbers of RPA foci on the outside of the paired chromo-

somes, implying residual ssDNA in aberrant configuration (Supplementary Figure S13). We also used SIM analysis to investigate the formation of long spike filaments by Dmc1. In RAD52-AID cells, as well as in RFA1-AID cells, but not in WT, we observed the presence of extended Dmc1-ssDNA spikes along the outer edges of the chromosome axes, resembling the RPA spike signals (Supplementary Figure S14).

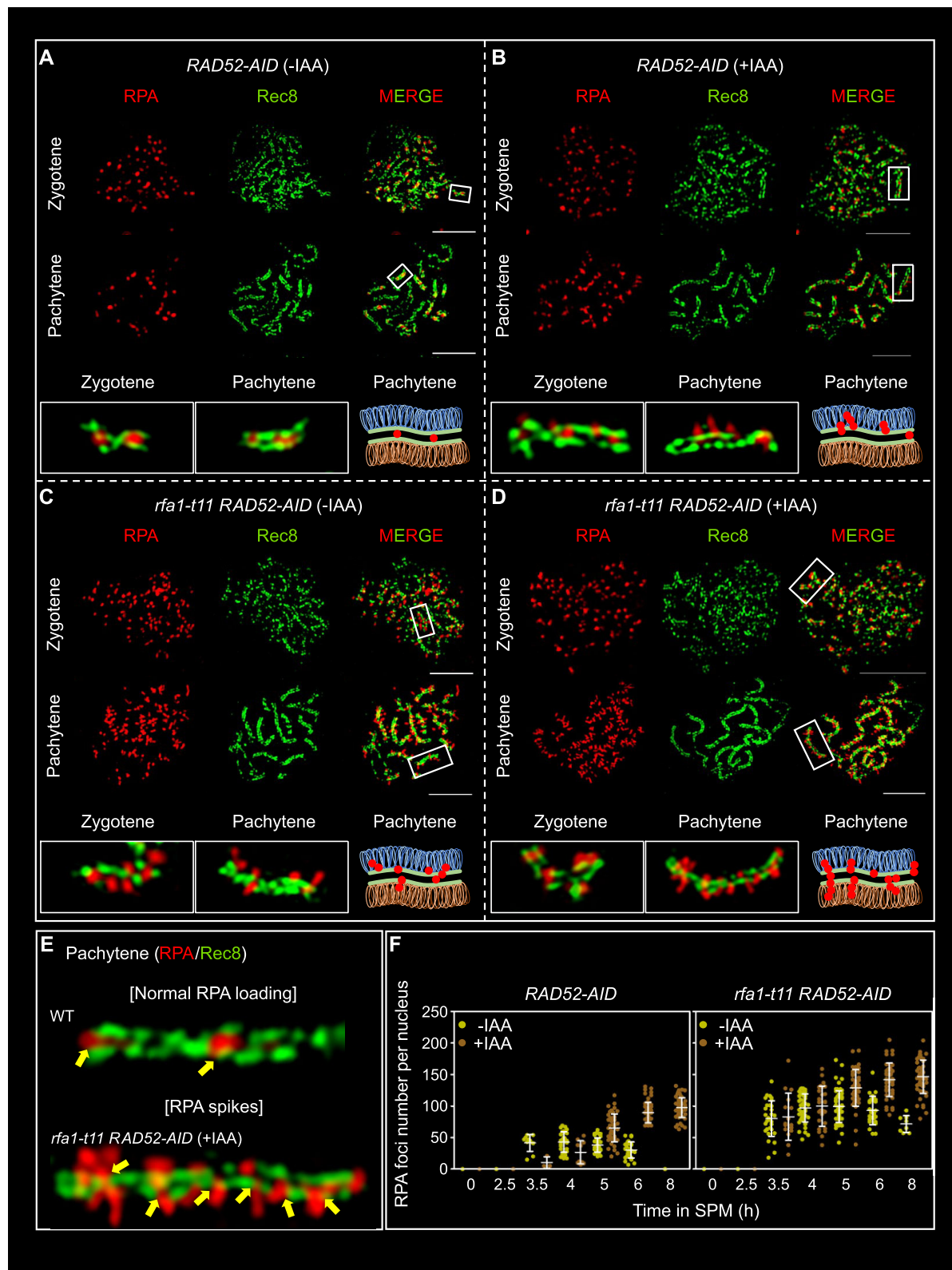


Figure 6. Arrangement of RPA-ssDNA on paired chromosomes in the presence or absence of Rad52. **(A–D)** Representative SIM images at zygote and pachytene chromosome. Auxin (2 mM) was added to induce degradation of Rad52 at 2.5 h. The cells were immunostained with anti-RPA and anti-HA (for Rec8-3HA) in spread chromosomes. Boxed regions from Rfa1-Rec8 co-staining images enlarged in (A–D). The scale bar represents 2.5 μ m. **(E)** ssDNA-bound RPA on the pachytene chromosomes. The arrows indicate the regions of abundance for RPA-ssDNA. **(F)** Number of RPA foci per nucleus in *RAD52-AID* and *rfa1-t11 RAD52-AID* strains. Data are presented as the mean \pm SD ($N \geq 20$).

During meiosis in the absence of either Rad51 or Dmc1, RPA foci form on chromosomes but fail to disappear normally (72) (Supplementary Figure S15A and B). Presumably, RPA forms on ssDNA tails while later stages of recombination are required for turnover. In the absence of either RecA homolog, SC formation is defective (22,73). However, a subset of chromosomes eventually reaches a pachytene-like stage, suggesting that CO/NCO differentiation can sometimes occur. SIM analysis further shows that, in the absence of either Dmc1 or RAD51, displacement of RPA from ssDNA is impaired in Rad52-RPA interaction mutants. The spike RPA filaments, somewhat distinct from *rfa1-t11* and *rad52** mutants, are positioned on pachytene-like chromosomes in *dmc1Δ*, showing defective SC, suggesting the persistent accumulation of unrepaired DSBs (Supplementary Figure S15C). These observations show that, in the absence of a RecA homolog, RPA is effectively localized to the recombination sites but its displacement from ssDNA is further impaired in the *rfa1-t11* or *rad52** cells.

Discussion

During meiotic recombination, physical and functional interaction of RPA and Rad52 is important for loading Rad51, thereby enabling its auxiliary functions. The present study identifies additional roles of this interaction at multiple later steps which are important for normal completion of both CO and NCO processes *in vivo*.

RPA interacts with RAD52 to mediate second end capture

The mutant phenotypes observed herein demonstrated that Rad52-RPA joint activity could mediate recombinational interaction regardless of whether strand exchange is carried out by Dmc1 or Rad51. Previous reports have highlighted the necessity of Rad51 in meiosis, as it is required for the recruitment of Dmc1 and the formation of a functional Rad51-Dmc1 filament (28,73). In our study, we observed the presence of Rad51 and Dmc1 foci in *rad52* and *rfa1* mutants, suggesting that the collaborative activity of Rad52-RPA is involved in the subsequent stages following strand invasion. Mutations that compromise the physical interaction between Rad51 and Rad52 exhibit a strong defect in progression of CO-fated SEIs to dHJs, with differential effect on IH-dHJs, and strong defects in formation of both COs and NCOs, with a differential effect on NCOs (18). These defects correspond to those attributed to the defect in second end capture originally defined for Rad52 (13,18) (Figure 7A). Along the CO pathway, the second end capture defect is seen directly in defective SEI-to-dHJ progression. SEIs that fail to do second end capture can then progress to a three-armed SEI which can then be resolved into half COs plus a broken end, giving some residual COs (18). In contrast, along the NCO pathway, the first end is released from its partner prior to second end capture; as a result, failure of second end capture will eliminate completely product formation. However, we cannot rule out the possibility that the reduced CO/NCO levels could also be explained by an earlier defect in strand invasion, including a delay in searching for homology, that occurs prior to the defect in the SEI-to-dHJ transition. We further find that timed degradation of RPA, when SEI formation has just begun in some nuclei, confers a near-total block in SEI-to dHJ formation. This de-

fect is not observed in absence of Rad52 and thus may reflect additional roles of RPA (further discussion below). However, a subset of cells (presumably those that have completed SEI formation at the time of inactivation) exhibit the same differential effects on IH- vs IS-dHJs and NCOs vs COs that correlate with a defect in second end capture. These effects are not attributable to the known early role of this interaction for loading Rad51 (so-called mediator function) because Rad51 foci occur normally in these mutants and because mediator function is not required for progression of SEIs to dHJs (18). It is unclear why the Rad52-RPA interaction is differentially required for formation of IH-dHJs versus IS-dHJs. Perhaps backup strand annealing pathway(s) exist for IS events. Interestingly, however, a mediator-proficient *rad52* mutant and the three interaction-defective mutants analyzed here are reduced in the IH:IS dHJ ratio. This phenotype has been observed previously in several other mutants and was proposed to reflect randomization of events at the two ends due to a defect in second end capture (10), although randomization at the DSB-to-SEI step is not excluded.

DSB resection and spike RPA in *rfa1* and *rad52* mutants

The Rad52-RPA interaction mutants show dramatic hyperresection of DSBs at the DNA level and, by cytological analysis, show elongated spikes of RPA that occur specifically at sites of recombination. Both of these phenotypes are easily accommodated by absence of second end capture. While one DSB end undergoes extensive strand invasion and extension, the other remains unaltered until second end capture (Figure 7A). Thus, DSB turnover effects may reflect alterations at both DSB ends. We also observe a modest defect in DSB turnover in the three interaction mutants. Such a delay also observed in *rad52Δ* mutant but is not in a *rad52* mutant lacking only mediator function, implying a non-mediator role (18). Absence of second end capture might be expected to result in a more dramatic accumulation of DSBs. Failure to observe this phenotype may be a consequence of the fact that DSB levels were defined in 1D gels, where hyperresection will cause most DSBs to migrate in a continuous smear rather than in the area corresponding to normal DSBs. Alternatively, or in addition, delayed turnover of the DSBs reflected in 1D gel analysis may be related to the delayed appearance of SEIs seen in the Rad52-RPA interaction mutant.

Spike RPA-ssDNA filament signals are more abundantly accumulated in the *rfa1-t11 rad52** mutant compared to each single mutant. To determine whether the spike RPA observed in *rfa1* and *rad52* mutants corresponds to the first DSB strand and/or the uncaptured second end, we evaluated the following experimental evidence: (i) Physical analysis of DNA showed that *rfa1-t11*, *rad52** and *RAD52-AID* mutants exhibit similar levels of DSB and SEI to those of the WT, while dHJ/CO and NCO levels decrease. In addition, SEIs undergo turnover and disappear in the mutants, suggesting that the spike RPA observed in the completed pachytene SC indicates an uncaptured DSB end or the first DSB end that has undergone strand disassembly, rather than SEI-to-dHJ or D-loop-to-NCO conversion (proposed model shown in Figure 7A). (ii) We observed WT numbers of Zip3 foci, representing CO-designated sites and CO-intermediates (SEIs), in *rfa1-t11* and *rad52** mutants. (iii) Specifically, in *rfa1* and *rad52* mutants, a significant amount of RPA foci was still observed even at late

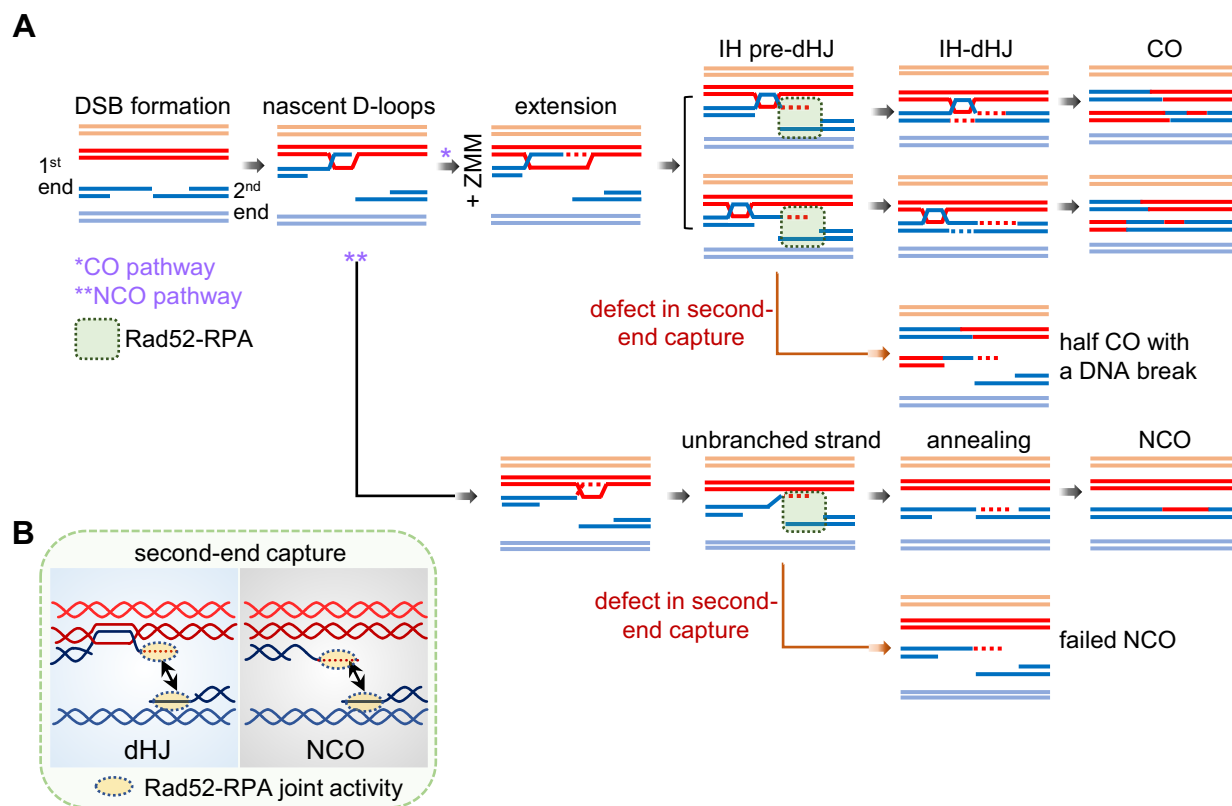


Figure 7. Model for roles of Rad52-RPA in meiotic DSB repair. **(A)** Defects in Rad52-RPA association at the second-end capture step result in a failure to form a canonical dHJ and/or NCO, and this reaction subsequently leads to a reduction in CO/NCO formation and an unrepaired-chromatid. The three-arm SEI could be formed by end-first displacement of the invading 3' end and migrating of the HJs into the dsDNA region (18). **(B)** Second end capture in meiotic recombination. RPA coats the leading DSB strands and the lagging DSB ends to mediate second end annealing through Rad52-catalytic activity. Annealing of the two DSB-ends via Rad52-RPA joint activity yields an IH-dHJ or a NCO.

pachytene. (iv) A significant increase in RPA levels was observed in *dmc1Δ* mutants, similar to the observations in *rfa1t11*, *rad52** and *RAD52-AID* mutants. Therefore, we suggest that spike RPA signal along the paired chromosomes in pachytene corresponds to the ends of the leading and/or lagging strands that have not undergone annealing after SEI/DSB loop formation.

Rad52–RPA interaction is important for timely SEI formation

The three interaction-defective mutants exhibit a delay in SEI formation, pointing to a defect after Rad51 loading and prior to emergence of stable/extensive strand invasion products along the CO pathway. RPA has been shown to occur at sites between/adjacent to resected DSB ends, leading to the proposition that it loads to the ssDNA created by D-loop formation (61,62). Perhaps an interaction with Rad52 is required at this stage. In contrast, the other event of this period, CO/NCO differentiation, appears to be unaffected because RPA spikes form specifically at CO sites in the three mutants, at approximately normal numbers.

RPA signals mark released DSB ends from TLACs

Spatial, temporal, and functional coordination of local events at the DNA/chromatin and axis levels is achieved via direct physical association of recombination complexes ('recombinosomes') with their underlying chromosome axes (74). Molecular studies have demonstrated that this association

arises via so-called 'tethered loop-axis complexes' (TLACs) in which recombinosomes that are organizationally situated in chromatin loops are, nonetheless, spatially associated with their underlying axes (10,74–76). Our findings demonstrate that RPA and Rec8 exhibit distinct patterns of loading along chromosome axes at the pachytene stage and that RPA regions on the axes are often depleted of Rec8 foci. This observation suggests that the distinct compartments along chromosomes in the early stage of meiotic recombination occur through two potential mechanisms: (i) DSB/RPA-rich regions correlate with domains with Red1/Hop1-rich regions that lack Rec8 (10) and (ii) Rec8 depletion is apparently required to release DSB ends from TLACs and to ensure that Dmc1/Rad51-coated DSBs search for homolog templates (10,77). Thus, Rad52-RPA joint activity is an important mediator of meiotic DSB repair events occurring in interaction with underlying chromosome axes.

RPA localization in mammal and plants

Immunofluorescence analyses of RPA performed in mammals and plants have demonstrated the occurrence of RPA foci up to the pachytene stage, specifically in association with SCs in the early and later meiotic prophase I, until MLH1 foci formation at the CO-fated recombination site (56,78–81). Analysis of *Arabidopsis* RPA mutants (*AtRPA1a*) has revealed that RPA is associated with meiotic chromosomes from the leptotene through the early pachytene, and is required to form normal levels of COs, and that *AtRPA1a* loss could decrease

second-end capture efficiency (79). Furthermore, the replacement of RPA-MEIOB-SPATA22 by Rad51 might be required in mammals to complete presynaptic filament formation and to mediate second-strand annealing (63,82). A previous study that conducted high-resolution *in vivo* mapping of RPA in mouse meiosis demonstrated that RPA/D-loops can be resolved as COs or NCOs (61). Therefore, RPA may have a recombination-specific role as a chaperone of ssDNA that coats the leading DSB end and the second DSB end to mediate second-end capture through a Rad52-catalytic activity (Figure 7B).

RPA contributes to meiotic recombination beyond its interplay with Rad52

Timed degradation of RPA at the SEI stage reveals two unexpected phenotypes: (i) a dramatic block at the SEI stage and (ii) for at least some of the intermediates that progress to the dHJ stage, a block to dHJ resolution. No such phenotypes are observed in a *rad52Δ* (18) or, in the present analysis, in any of the Rad52/RPA interaction mutants or upon timed degradation of RAD52. We infer that these phenotypes reflect unsuspected roles of RPA that do not involve its interaction with Rad52. RPA interacts with various DNA break repair proteins, including Mre11 and many other repair proteins, suggesting a functional role beyond its association with Rad52 (58,83). It has been reported that RPA is linked to the DNA/chromosome-based signal transduction kinase cascade triggered via ATR/ATM (Mec1/Tel1 in budding yeast), which are not only involved in damage surveillance but also in promoting the progression of recombination in WT meiosis (84). Thus, the degradation of RPA may potentially lead to a significantly pronounced checkpoint activation. Moreover, its association with MRX is important to hold sister chromatids together at spontaneous DSB sites independently of cohesion (58). Thus, the differential involvement of RPA likely also allows for the integration of these major types of interaction, thus enabling the coordination of axis-associated recombinosomes (10). To facilitate these processes, RPA could play important roles via its dynamics on ssDNA, including timely displacement by recombinases and interaction with recombination regulatory proteins.

Data availability

The data underlying this article are available in the article and in its online supplementary material.

Supplementary data

[Supplementary Data](#) are available at NAR Online.

Acknowledgements

We would like to express our gratitude to Richard Kolodner and Alain Nicolas for providing the plasmids and strains used in this study, as well as to Liangran Zhang for sharing unpublished data.

Funding

National Research Foundation of Korea (NRF) grant funded by the Korea government (MSIT) [2018R1A5A1025077,

2021R1I1A1A01059573, 2022R1I1A1A01055532, 2022M3A9J4079468, RS-2023-00208191]; Kun-hee Lee Seoul National University Hospital Child Cancer & Rare Disease Project, Republic of Korea [22B-001-0500]; N.K. also received support from the U.S. National Institutes of Health [R35-GM-136322].

Conflict of interest statement

None declared.

References

1. Hunter,N. (2015) Meiotic recombination: the essence of heredity. *Cold Spring Harb. Perspect. Biol.*, **7**, a016618.
2. Zickler,D. and Kleckner,N. (2015) Recombination, pairing, and synapsis of homologs during meiosis. *Cold Spring Harb. Perspect. Biol.*, **7**, a016626.
3. Hong,S., Joo,J.H., Yun,H. and Kim,K.P. (2019) The nature of meiotic chromosome dynamics and recombination in budding yeast. *J. Microbiol.*, **57**, 221–231.
4. de Massy,B. (2013) Initiation of meiotic recombination: how and where? Conservation and specificities among eukaryotes. *Annu. Rev. Genet.*, **47**, 563–599.
5. Garcia,V., Phelps,S.E., Gray,S. and Neale,M.J. (2011) Bidirectional resection of DNA double-strand breaks by Mre11 and Exo1. *Nature*, **479**, 241–244.
6. Keeney,S., Lange,J. and Mohibullah,N. (2014) Self-organization of meiotic recombination initiation: general principles and molecular pathways. *Annu. Rev. Genet.*, **48**, 187–214.
7. Mimitou,E.P. and Symington,L.S. (2008) Sae2, Exo1 and Sgs1 collaborate in DNA double-strand break processing. *Nature*, **455**, 770–774.
8. Neale,M.J., Pan,J. and Keeney,S. (2005) Endonucleolytic processing of covalent protein-linked DNA double-strand breaks. *Nature*, **436**, 1053–1057.
9. Zakharyevich,K., Ma,Y., Tang,S., Hwang,P.Y., Boiteux,S. and Hunter,N. (2010) Temporally and biochemically distinct activities of Exo1 during meiosis: double-strand break resection and resolution of double Holliday junctions. *Mol. Cell*, **40**, 1001–1015.
10. Kim,K.P., Weiner,B.M., Zhang,L., Jordan,A., Dekker,J. and Kleckner,N. (2010) Sister cohesion and structural axis components mediate homolog bias of meiotic recombination. *Cell*, **143**, 924–937.
11. Hong,S., Sung,Y., Yu,M., Lee,M., Kleckner,N. and Kim,K.P. (2013) The logic and mechanism of homologous recombination partner choice. *Mol. Cell*, **51**, 440–453.
12. Storlazzi,A., Gargano,S., Ruprich-Robert,G., Falque,M., David,M., Kleckner,N. and Zickler,D. (2010) Recombination proteins mediate meiotic spatial chromosome organization and pairing. *Cell*, **141**, 94–106.
13. Ahuja,J.S., Harvey,C.S., Wheeler,D.L. and Lichten,M. (2021) Repeated strand invasion and extensive branch migration are hallmarks of meiotic recombination. *Mol. Cell*, **81**, 4258–4270.
14. Allers,T. and Lichten,M. (2001) Differential timing and control of noncrossover and crossover recombination during meiosis. *Cell*, **106**, 47–57.
15. Börner,G.V., Kleckner,N. and Hunter,N. (2004) Crossover/noncrossover differentiation, synaptonemal complex formation, and regulatory surveillance at the leptotene/zygotene transition of meiosis. *Cell*, **117**, 29–45.
16. Martini,E., Diaz,R.L., Hunter,N. and Keeney,S. (2006) Crossover homeostasis in yeast meiosis. *Cell*, **126**, 285–295.
17. Hunter,N. and Kleckner,N. (2001) The single-end invasion: an asymmetric intermediate at the double-strand break to double-holliday junction transition of meiotic recombination. *Cell*, **106**, 59–70.

- 18.** Lao,J.P., Oh,S.D., Shinohara,M., Shinohara,A. and Hunter,N. (2008) Rad52 promotes postinvasion steps of meiotic doublestrand-break repair. *Mol. Cell*, **29**, 517–524.
- 19.** Zickler,D. and Kleckner,N. (2023) Meiosis: dances between homologs. *Annu. Rev. Genet.*, **57**, 1–63.
- 20.** Oh,S.D., Lao,J.P., Hwang,P.Y., Taylor,A.F., Smith,G.R. and Hunter,N. (2007) BLM ortholog, Sgs1, prevents aberrant crossing-over by suppressing formation of multichromatid joint molecules. *Cell*, **130**, 259–272.
- 21.** Crickard,J.B., Kaniecki,K., Kwon,Y., Sung,P. and Greene,E.C. (2018) Spontaneous self-segregation of Rad51 and Dmc1 DNA recombinases within mixed recombinase filaments. *J. Biol. Chem.*, **293**, 4191–4200.
- 22.** Hayase,A., Takagi,M., Miyazaki,T., Oshiumi,H., Shinohara,M. and Shinohara,A. (2004) A protein complex containing Mei5 and Sae3 promotes the assembly of the meiosis-specific RecA homolog Dmc1. *Cell*, **119**, 927–940.
- 23.** Kim,K.P. and Mirkin,E.V. (2018) So similar yet so different: the two ends of a double strand break. *Mutat. Res.*, **809**, 70–80.
- 24.** Kurzbauer,M.T., Uanschou,C., Chen,D. and Schlögelhofer,P. (2012) The recombinases DMC1 and RAD51 are functionally and spatially separated during meiosis in Arabidopsis. *Plant Cell*, **24**, 2058–2070.
- 25.** Peterson,S.E., Keeney,S. and Jasin,M. (2020) Mechanistic insight into crossing over during mouse meiosis. *Mol. Cell*, **78**, 1252–1263.
- 26.** Sheridan,S.D., Yu,X., Roth,R., Heuser,J.E., Sehorn,M.G., Sung,P., Egelman,E.H. and Bishop,D.K. (2008) A comparative analysis of Dmc1 and Rad51 nucleoprotein filaments. *Nucleic Acids Res.*, **36**, 4057–4066.
- 27.** Lao,J.P., Cloud,V., Huang,C.C., Grubb,J., Thacker,D., Lee,C.Y., Dresser,M.E., Hunter,N. and Bishop,D.K. (2013) Meiotic crossover control by concerted action of Rad51-Dmc1 in homolog template bias and robust homeostatic regulation. *PLoS Genet.*, **9**, e1003978.
- 28.** Cloud,V., Chan,Y.-L., Grubb,J., Budke,B. and Bishop,D.K. (2012) Rad51 is an accessory factor for Dmc1-mediated joint molecule formation during meiosis. *Science*, **337**, 1222–1225.
- 29.** Binz,S.K. and Wold,M.S. (2008) Regulatory functions of the N-terminal domain of the 70-kDa subunit of replication protein A (RPA). *J. Biol. Chem.*, **283**, 21559–21570.
- 30.** Iftode,C., Daniely,Y. and Borowiec,J.A. (1999) Replication protein A (RPA): the eukaryotic SSB. *Crit. Rev. Biochem. Mol. Biol.*, **34**, 141–180.
- 31.** Soustelle,C., Vedel,M., Kolodner,R. and Nicolas,A. (2002) Replication protein A is required for meiotic recombination in *Saccharomyces cerevisiae*. *Genetics*, **161**, 535–547.
- 32.** Wold,M.S. (1997) Replication protein A: a heterotrimeric, single-stranded DNA-binding protein required for eukaryotic DNA metabolism. *Annu. Rev. Biochem.*, **66**, 61–92.
- 33.** Yates,I.A., Aramayo,R.J., Pokhrel,N., Caldwell,C.C., Kaplan,J.A., Perera,R.L., Spies,M., Antony,E. and Zhang,X. (2018) A structural and dynamic model for the assembly of Replication Protein A on single-stranded DNA. *Nat. Commun.*, **9**, 5447.
- 34.** Deveryshtetty,J., Chadda,R., Mattice,J.R., Karunakaran,S., Rau,M.J., Basore,K., Pokhrel,N., Englander,N., Fitzpatrick,J.A.J., Bothner,B., et al. (2023) Yeast Rad52 is a homodecamer and possesses BRCA2-like bipartite Rad51 binding modes. *Nat. Commun.*, **14**, 6215.
- 35.** Dubrana,K., van Attikum,H., Hediger,F. and Gasser,S.M. (2007) The processing of double-strand breaks and binding of single-strand-binding proteins RPA and Rad51 modulate the formation of ATR-kinase foci in yeast. *J. Cell Sci.*, **120**, 4209–4220.
- 36.** Shinohara,A., Shinohara,M., Ohta,T., Matsuda,S. and Ogawa,T. (1998) Rad52 forms ring structures and cooperates with RPA in single-strand DNA annealing. *Genes Cells*, **3**, 145–156.
- 37.** Sugiyama,T., Kantake,N., Wu,Y. and Kowalczykowski,S.C. (2006) Rad52-mediated DNA annealing after Rad51-mediated DNA strand exchange promotes second ssDNA capture. *EMBO J.*, **25**, 5539–5548.
- 38.** Sugiyama,T. and Kowalczykowski,S.C. (2002) Rad52 protein associates with replication protein A (RPA)-single-stranded DNA to accelerate Rad51-mediated displacement of RPA and presynaptic complex formation. *J. Biol. Chem.*, **277**, 31663–31672.
- 39.** Stauffer,M.E. and Chazin,W.J. (2004) Physical interaction between replication protein A and Rad51 promotes exchange on single-stranded DNA. *J. Biol. Chem.*, **279**, 25638–25645.
- 40.** Ma,C.J., Gibb,B., Kwon,Y., Sung,P. and Greene,E.C. (2017) Protein dynamics of human RPA and RAD51 on ssDNA during assembly and disassembly of the RAD51 filament. *Nucleic Acids Res.*, **45**, 749–761.
- 41.** Pokhrel,N., Caldwell,C.C., Corless,E.I., Tillison,E.A., Tibbs,J., Jocic,N., Tabei,S.M.A., Wold,M.S., Spies,M. and Antony,E. (2019) Dynamics and selective remodeling of the DNA-binding domains of RPA. *Nat. Struct. Mol. Biol.*, **26**, 129–136.
- 42.** Nimonkar,A.V., Sica,R.A. and Kowalczykowski,S.C. (2009) Rad52 promotes second-end DNA capture in double-stranded break repair to form complement-stabilized joint molecules. *Proc. Natl. Acad. Sci. U.S.A.*, **106**, 3077–3082.
- 43.** Lim,G., Chang,Y. and Huh,W.K. (2020) Phosphoregulation of Rad51/Rad52 by CDK1 functions as a molecular switch for cell cycle-specific activation of homologous recombination. *Sci. Adv.*, **6**, eaay2669.
- 44.** McIlwraith,M.J. and West,S.C. (2008) DNA repair synthesis facilitates RAD52-mediated second-end capture during DSB repair. *Mol. Cell*, **29**, 510–516.
- 45.** Plate,I., Hallwyl,S.C., Shi,I., Krejci,L., Müller,C., Albertsen,L. and Mortensen,U.H. (2008) Interaction with RPA is necessary for Rad52 repair center formation and for its mediator activity. *J. Biol. Chem.*, **283**, 29077–29085.
- 46.** Sugiyama,T. and Kantake,N. (2009) Dynamic regulatory interactions of rad51, rad52, and replication protein-a in recombination intermediates. *J. Mol. Biol.*, **390**, 45–55.
- 47.** Sugiyama,T., New,J.H. and Kowalczykowski,S.C. (1998) DNA annealing by RAD52 protein is stimulated by specific interaction with the complex of replication protein A and single-stranded DNA. *Proc. Natl. Acad. Sci. U.S.A.*, **95**, 6049–6054.
- 48.** Cho,H.R., Kong,Y.J., Hong,S.G. and Kim,K.P. (2016) Hop2 and Sae3 are required for Dmc1-mediated double-strand break repair via homolog bias during meiosis. *Mol. Cells*, **39**, 550–556.
- 49.** Kong,Y.J., Joo,J.H., Kim,K.P. and Hong,S. (2017) Hed1 promotes meiotic crossover formation in *Saccharomyces cerevisiae*. *J. Microbiol. Biotechnol.*, **27**, 405–411.
- 50.** Yoon,S.W., Lee,M.S., Xaver,M., Zhang,L., Hong,S.G., Kong,Y.J., Cho,H.R., Kleckner,N. and Kim,K.P. (2016) Meiotic prophase roles of Rec8 in crossover recombination and chromosome structure. *Nucleic Acids Res.*, **44**, 9296–9314.
- 51.** Joo,J.H., Kang,H.A., Kim,K.P. and Hong,S. (2022) Meiotic prophase roles of Pds5 in recombination and chromosome condensation in budding yeast. *J. Microbiol.*, **60**, 177–186.
- 52.** Lee,M.S., Higashide,M.T., Choi,H., Li,K., Hong,S., Lee,K., Shinohara,A., Shinohara,M. and Kim,K.P. (2021) The synaptonemal complex central region modulates crossover pathways and feedback control of meiotic double-strand break formation. *Nucleic Acids Res.*, **49**, 7537–7553.
- 53.** Loidl,J., Klein,F. and Engebrecht,J. (1998) Genetic and morphological approaches for the analysis of meiotic chromosomes in yeast. *Methods Cell Biol.*, **53**, 257–285.
- 54.** Shinohara,M., Gasior,S.L., Bishop,D.K. and Shinohara,A. (2000) Tid1/Rdh54 promotes colocalization of rad51 and dmc1 during meiotic recombination. *Proc. Natl. Acad. Sci. U.S.A.*, **97**, 10814–10819.
- 55.** Gerace,E. and Moazed,D. (2014) Coimmunoprecipitation of proteins from yeast. *Methods Enzymol.*, **541**, 13–26.
- 56.** Yoon,S., Choi,E.H., Kim,J.W. and Kim,K.P. (2018) Structured illumination microscopy imaging reveals localization of replication

- protein A between chromosome lateral elements during mammalian meiosis. *Exp. Mol. Med.*, **50**, 1–12.
57. Sasanuma,H., Hirota,K., Fukuda,T., Kakusho,N., Kugou,K., Kawasaki,Y., Shibata,T., Masai,H. and Ohta,K. (2008) Cdc7-dependent phosphorylation of Mer2 facilitates initiation of yeast meiotic recombination. *Genes. Dev.*, **22**, 398–410.
58. Seeber,A., Hegnauer,A.M., Hustedt,N., Deshpande,I., Poli,J., Eglinger,J., Pasero,P., Gut,H., Shinohara,M. and Hopfner,K.P. (2016) RPA mediates recruitment of MRX to forks and double-strand breaks to hold sister chromatids together. *Mol. Cell*, **64**, 951–966.
59. Kantake,N., Sugiyama,T., Kolodner,R.D. and Kowalczykowski,S.C. (2003) The recombination-deficient mutant RPA (rfa1-t11) is displaced slowly from single-stranded DNA by Rad51 protein. *J. Biol. Chem.*, **278**, 23410–23417.
60. Hegnauer,A.M., Hustedt,N., Shimada,K., Pike,B.L., Vogel,M., Amsler,P., Rubin,S.M., van Leeuwen,F., Guénolé,A., van Attikum,H., et al. (2012) An N-terminal acidic region of Sgs1 interacts with Rpa70 and recruits Rad53 kinase to stalled forks. *EMBO J.*, **31**, 3768–3783.
61. Hinch,A.G., Becker,P.W., Li,T., Moralli,D., Zhang,G., Bycroft,C., Green,C., Keeney,S., Shi,Q., Davies,B., et al. (2020) The configuration of RPA, RAD51, and DMC1 binding in meiosis reveals the nature of critical recombination Intermediates. *Mol. Cell*, **79**, 689–701.
62. Wang,X. and Haber,J.E. (2004) Role of Saccharomyces single-stranded DNA-binding protein RPA in the strand invasion step of double-strand break repair. *PLoS Biol.*, **2**, E21.
63. Shi,B., Xue,J., Yin,H., Guo,R., Luo,M., Ye,L. and Wang,P.J. (2019) Dual functions for the ssDNA-binding protein RPA in meiotic recombination. *PLoS Genet.*, **15**, e1007952.
64. Fung,J.C., Rockmill,B., Odell,M. and Roeder,G.S. (2004) Imposition of crossover interference through the nonrandom distribution of synapsis initiation complexes. *Cell*, **116**, 795–802.
65. Serrentino,M.E., Chaplais,E., Sommermeyer,V. and Borde,V. (2013) Differential association of the conserved SUMO ligase Zip3 with meiotic double-strand break sites reveals regional variations in the outcome of meiotic recombination. *PLoS Genet.*, **9**, e1003416.
66. de los Santos,T., Hunter,N., Lee,C., Larkin,B., Loidl,J. and Hollingsworth,N.M. (2003) The Mus81/Mms4 endonuclease acts independently of double-Holliday junction resolution to promote a distinct subset of crossovers during meiosis in budding yeast. *Genetics*, **164**, 81–94.
67. De Muyt,A., Pyatnitskaya,A., Andreani,J., Ranjha,L., Ramus,C., Laureau,R., Fernandez-Vega,A., Holoch,D., Girard,E., Govin,J., et al. (2018) A meiotic XPF–ERCC1-like complex recognizes joint molecule recombination intermediates to promote crossover formation. *Genes Dev.*, **32**, 283–296.
68. Lynn,A., Soucek,R. and Börner,G.V. (2007) ZMM proteins during meiosis: crossover artists at work. *Chromosome Res.*, **15**, 591–605.
69. Manhart,C.M. and Alani,E. (2016) Roles for mismatch repair family proteins in promoting meiotic crossing over. *DNA Repair (Amst.)*, **38**, 84–93.
70. Pyatnitskaya,A., Borde,V. and De Muyt,A. (2019) Crossing and zipping: molecular duties of the ZMM proteins in meiosis. *Chromosoma*, **128**, 181–198.
71. Shinohara,M., Oh,S.D., Hunter,N. and Shinohara,A. (2008) Crossover assurance and crossover interference are distinctly regulated by the ZMM proteins during yeast meiosis. *Nat. Genet.*, **40**, 299–309.
72. Gasior,S.L., Wong,A.K., Kora,Y., Shinohara,A. and Bishop,D.K. (1998) Rad52 associates with RPA and functions with rad55 and rad57 to assemble meiotic recombination complexes. *Genes. Dev.*, **12**, 2208–2221.
73. Reitz,D., Grubb,J. and Bishop,D.K. (2019) A mutant form of Dmc1 that bypasses the requirement for accessory protein Mei5-Sae3 reveals independent activities of Mei5-Sae3 and Rad51 in Dmc1 filament stability. *PLoS Genet.*, **15**, e1008217.
74. Kleckner,N. (2006) Chiasma formation: chromatin/axis interplay and the role(s) of the synaptonemal complex. *Chromosoma*, **115**, 175–194.
75. Blat,Y., Protacio,R.U., Hunter,N. and Kleckner,N. (2002) Physical and functional interactions among basic chromosome organizational features govern early steps of meiotic chiasma formation. *Cell*, **111**, 791–802.
76. Panizza,S., Mendoza,M.A., Berlinger,M., Huang,L., Nicolas,A., Shirahige,K. and Klein,F. (2011) Spo11-accessory proteins link double-strand break sites to the chromosome axis in early meiotic recombination. *Cell*, **146**, 372–383.
77. Shinohara,M., Hayashihara,K., Grubb,J.T., Bishop,D.K. and Shinohara,A. (2015) DNA damage response clamp 9-1-1 promotes assembly of ZMM proteins for formation of crossovers and synaptonemal complex. *J. Cell Sci.*, **128**, 1494–1506.
78. Moens,P.B., Kolas,N.K., Tarsounas,M., Marcon,E., Cohen,P.E. and Spyropoulos,B. (2002) The time course and chromosomal localization of recombination-related proteins at meiosis in the mouse are compatible with models that can resolve the early DNA-DNA interactions without reciprocal recombination. *J. Cell Sci.*, **115**, 1611–1622.
79. Osman,K., Sanchez-Moran,E., Mann,S.C., Jones,G.H. and Franklin,F.C. (2009) Replication protein A (AtRPA1a) is required for class I crossover formation but is dispensable for meiotic DNA break repair. *EMBO J.*, **28**, 394–404.
80. Plug,A.W., Peters,A.H., Keegan,K.S., Hoekstra,M.F., de Boer,P. and Ashley,T. (1998) Changes in protein composition of meiotic nodules during mammalian meiosis. *J. Cell Sci.*, **111**, 413–423.
81. Woglar,A. and Villeneuve,A.M. (2018) Dynamic architecture of DNA repair complexes and the synaptonemal complex at sites of meiotic recombination. *Cell*, **173**, 1678–1691.
82. Luo,M., Yang,F., Leu,N.A., Landache,J., Handel,M.A., Benavente,R., La Salle,S. and Wang,P.J. (2013) MEIOB exhibits single-stranded DNA-binding and exonuclease activities and is essential for meiotic recombination. *Nat. Commun.*, **4**, 2788.
83. Zou,L. and Elledge,S.J. (2003) Sensing DNA damage through ATRIP recognition of RPA-ssDNA complexes. *Science*, **300**, 1542–1548.
84. Hochwagen,A. and Amon,A. (2006) Checking your breaks: surveillance mechanisms of meiotic recombination. *Curr. Biol.*, **16**, R217–R228.
85. Umez,K., Sugawara,N., Chen,C., Haber,J.E. and Kolodner,R.D. (1998) Genetic analysis of yeast RPA1 reveals its multiple functions in DNA metabolism. *Genetics*, **148**, 989–1005.